Simulation Studies of Amide I IR Absorption and Two-Dimensional IR Spectra of β Hairpins in Liquid Water

Seungsoo Hahn,[†] Sihyun Ham,[‡] and Minhaeng Cho*[,†]

Department of Chemistry and Center for Multidimensional Spectroscopy, Division of Chemistry and Molecular Engineering, Korea University, Seoul 136-701, Korea, and Department of Chemistry, Sookmyung Women's University, Seoul 140-742, Korea

Received: January 25, 2005; In Final Form: April 11, 2005

Amide I IR absorption and two-dimensional (2D) IR photon echo spectra of a model β hairpin in aqueous solution are theoretically studied and simulated by combining semiempirical quantum chemistry calculations and molecular dynamics simulation methods. The instantaneous normal-mode analysis of the β hairpin in solution is performed to obtain the density of states and the inverse participation ratios of the one-exciton states. The motional and exchange narrowing processes are taken into account by employing the time-correlation function theory for the linear and nonlinear response functions. Numerically simulated IR absorption and 2D spectra are then found to be determined largely by the amide I normal modes delocalized on the peptides in the two strands. The site-specific isotope-labeling effects on the IR and 2D IR spectra are discussed. The simulation results for the ideal (A_{17}) β hairpin are directly compared with those of the realistic 16-residue (GB1) β hairpin from an immunoglobulin G-binding protein. It was found that the characteristic features in IR and 2D spectra of both the ideal (A_{17}) β hairpin and the GB1 β hairpin are the same. The simulated IR spectrum of the GB1 β hairpin is found to be in good agreement with experiment, which demonstrates that the present computational method is quantitatively reliable.

I. Introduction

The primary sequence of a given protein contains crucial information about the 3D structure that is mainly the determining factor specifying its biological function.[1] To understand how the primary sequence folds into the functional structure, we carried out a number of experiments and molecular dynamics simulations for peptide fragments.[2−9] Also, the mutation effects on the stability of a given protein have been studied extensively by monitoring its structural and functional changes.[10−13]

Among the various secondary-structure polypeptides, the β-hairpin motif containing two antiparallel β-strands that are connected to each other by a turn or loop has been studied extensively because it is the smallest antiparallel β-sheet system.[4] Despite their small size (typically less than 20 residues), those β hairpins exhibit various properties that are typical in globular proteins.[9] One of the most extensively studied β hairpins is the *C*-terminal fragment of the protein GB1 domain with 16 residues, and its cooperative thermal folding−unfolding transition behavior was observed.[14−17] Moreover, it was shown that the β hairpin can serve as a nucleation site at an early stage of folding events.[18−20] Thus, the β hairpin itself has drawn much attention in terms of investigating the protein folding mechanism.

By analyzing the IR spectra of the 16-residue β hairpin (GEWTYDDATKTFTVTE), which is the second β hairpin of the B1 domain of an immunoglobulin G-binding protein from group G *Streptococcus*, Arrondo et al.[21] found two characteristic features distinguishing its spectrum from that of an antiparallel β-sheet: (1) the low-frequency band of the β hairpin appears at 1620 cm^{-1}, whereas that of an antiparallel β-sheet is at 1632 cm^{-1}, and (2) the high-frequency peak does not undergo any isotopic shift in D_2O solvent, which is, in contrast, typical for an antiparallel β-sheet. Later, Colley et al.[22] observed no discernible feature in the amide I IR spectrum indicating any significant contribution from the interstrand hydrogen bonds at low concentrations (about 2 mM) of the 16-residue β hairpin (KKYTVSINGKKITVSI), even though at high concentrations (>10 mM) a new band at 1616 cm^{-1} appears, which is consistent with the onset of irreversible peptide aggregation. To understand the folding−unfolding time scale, Xu et al.[23] studied the thermal stability and folding kinetics of the 15-residue β hairpin (SESYINPDGTWTVTE) by employing the time-resolved infrared spectroscopy coupled with the laser-induced temperature-jump technique for rapid unfolding initiation. Probing the IR intensity change at 1634 cm^{-1}, they found that the folding of the β hairpin follows first-order kinetics and is relatively fast, $\sim$0.8 μs at 300 K.

Despite the fact that the infrared (IR) spectroscopic techniques have been used extensively to obtain the structural information of numerous polypeptides and proteins in solutions, the 1D IR absorption measurement method, like all other linear spectroscopies, has an intrinsic limitation that the band shapes for different secondary structured polypeptides are similar to one another and highly spectrally congested. A number of spectroscopic methods have been proposed and used to eventually establish the general structure−spectra relationships in order to overcome this barrier potentially limiting the 1D IR method's applicability to structure determination of polypeptides in condensed phases. One notable advance along this line has been made in the fields of vibrational optical activity, such as vibrational circular dichroism and Raman optical activity

* To whom correspondence should be addressed. E-mail: mcho@korea.ac.kr.
[†] Korea University.
[‡] Sookmyung Women's University.

10.1021/jp050450j CCC: $30.25
Published on Web 05/19/2005

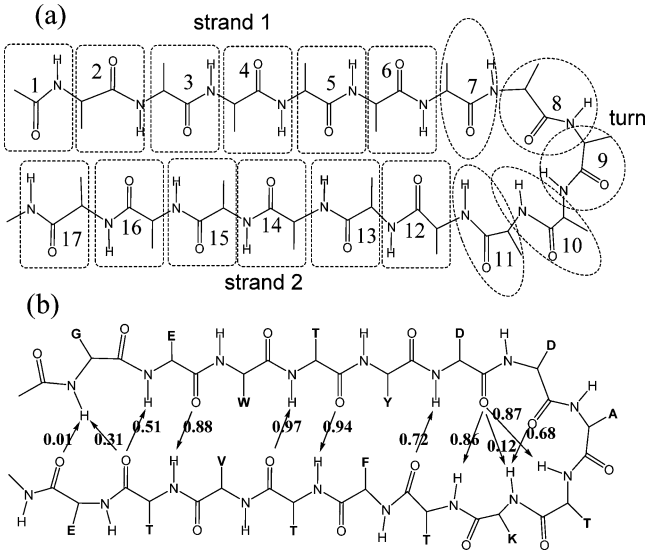

Figure 1. Molecular structures of alanine-based model β hairpin (a) consisting of 17 peptide bonds and of the GB1 β hairpin (b). In Figure 1b, the numbers correspond to the probability of finding the intramolecular hydrogen bond during the MD simulation trajectory.

spectroscopies. Although these two methods are also linear spectroscopies, they provide additional information on the angles between the transition dipoles of coupled local oscillators. Only recently, 2D vibrational spectroscopic methods have been shown to be useful in extracting the structural information of polypeptides[24−28] and nucleic acids[29] in condensed phases because they provide a means of studying the influence of the local conformation, hydrogen-bonding structure and dynamics, and structure-dependent couplings among relevant vibrational degrees of freedom. For example, Hochstrasser and co-workers used the 2D IR (photon echo) spectroscopic technique to obtain spectral characteristics of an α helix in liquid water, where they successfully described the origin of cross peaks and demonstrated the sensitivity of the 2D spectra on its 3D polypeptide structure.[24] Tokmakoff, Knoester, and co-workers performed similar 2D IR studies of various proteins containing a large amount of antiparallel β-sheets and observed the characteristic "Z"-shaped 2D spectra for the antiparallel β-sheet polypeptides.[25a] Knowing that the β hairpin can be viewed as a double-stranded antiparallel β-sheet polypeptide,[25b] one might expect the same 2D spectral pattern to be observed in the experiment. In the present work, we use various computational methods combining electronic structure calculations and molecular dynamics simulations to theoretically study the amide I density of states, the extent of delocalization, the motional and exchange narrowing processes, and the isotope-labeled effects on IR absorption and 2D vibrational spectra of the β hairpin in liquid water. In the present paper, we consider two different β hairpins, the ideal (model) β hairpin, denoted as the A_{17} β hairpin, consisting of 16 alanine amino acids and the more realistic β hairpin of the B1 domain of an immunoglobulin G-binding protein from group G *Streptococcus*, denoted as the GB1 β hairpin (see Figure 1). We will first discuss the general trends and characteristic features found in the amide I IR and 2D spectra of the A_{17} β hairpin and then compare them directly with those of the GB1 β hairpin.

II. Structure, Transition Dipoles, and Couplings in the A_{17} β Hairpin

The local amide I mode frequency is influenced by several factors such as intramolecular peptide−peptide interaction, the side-chain effect, and peptide−solvent interaction. In this section, we will present the Hessian matrix reconstruction (HMR) analysis results on the amide I vibrational properties of the isolated A_{17} β hairpin polypeptide, for example, the local and normal frequencies, vibrational coupling constants, and transition dipole moments. Second, the transition-dipole-weighted phase correlation factor is defined and is shown to be useful in investigating how both the vibrational coupling constants and the local mode transition dipole moments simultaneously contribute to the IR intensities and thus amide I band shape.

A. Frequency Scaling Scheme. To obtain the vibrational properties of the A_{17} β hairpin, we first performed geometry optimization and vibrational analysis using the semiempirical quantum chemistry calculation method (AM1). The validity of the AM1 approximation to compute the amide I vibrational properties have been studied recently in detail, and a proper frequency-scaling algorithm was developed. Comparing a series of AM1-calculated amide I frequencies of various polypeptides with those obtained with the HF/6-311++G** method, it was found that the proper scaling equation is given as $\tilde{\nu}_{\text{scaled}} = a + b\,(\tilde{\nu}_{\text{AM1}} - 1994.5)$ in cm^{-1}, where the two constants a and b are 1707.1 and 1.8 cm^{-1}, respectively.[30] $\tilde{\nu}_{\text{AM1}}$ on the right-hand side of this scaling equation is the unscaled AM1-calculated amide I *local* mode frequency. This scaling method was tested by directly comparing numerically the simulated IR absorption, the vibrational circular dichroism, and the 2D IR photon echo spectra of various isotope-labeled α helices in liquid water.[31]

We next discuss the generalized Hessian matrix reconstruction method to obtain the amide I local mode frequencies and vibrational coupling constants from the amide I normal-mode frequencies and corresponding eigenvectors in the atomic Cartesian coordinate system; note that the amide I normal-mode frequencies and eigenvectors are direct outputs of the AM1 vibrational analysis. Suppose that the eigenvector of the jth amide I local mode is fully determined by the eigenvector elements, in the Cartesian coordinate system, associated with the six atoms, O(=C), C(=O), N(−H), H(−N), C_α, and H(−C_α) that constitute the jth peptide bond. The corresponding eigenvector will be denoted as $U_{m,j}$, where m is the index of the Cartesian coordinates of the six atoms constituting the jth peptide bond. Then, we found that the Hessian matrix elements, force constants, can be obtained as

$$F_{ij} = \sum_{n,m} U^{-1}_{i,n} \bar{F}_{n,m} U_{m,j} \tag{1}$$

where $\bar{F}_{n,m}$ is the original Hessian matrix in the mass-weighted Cartesian coordinate system, which can be obtained directly from the quantum chemistry vibrational analysis of the entire polypeptide. F_{ij} is the Hessian matrix reconstructed in the amide I local mode subspace so that its diagonal and off-diagonal matrix elements correspond to the mass-weighted amide I local mode force constants and coupling force constants, respectively. The thus obtained amide I local mode frequencies are to be scaled by using the scaling equation mentioned above.

The local amide I mode frequencies are plotted in the upper panel of Figure 2, and the dihedral angles, ϕ_j and ψ_j, of the geometry optimized A_{17} β hairpin are plotted in the bottom panel. In this case of the isolated A_{17} β hairpin, the amide I local mode frequency is red-shifted when the carbonyl group forms a hydrogen bond with the H−N hydrogen atom of the peptide in another strand. The local amide I mode frequencies thus reflect this structural pattern of the alternating carbonyl group orientations along the β-hairpin backbone.[30]

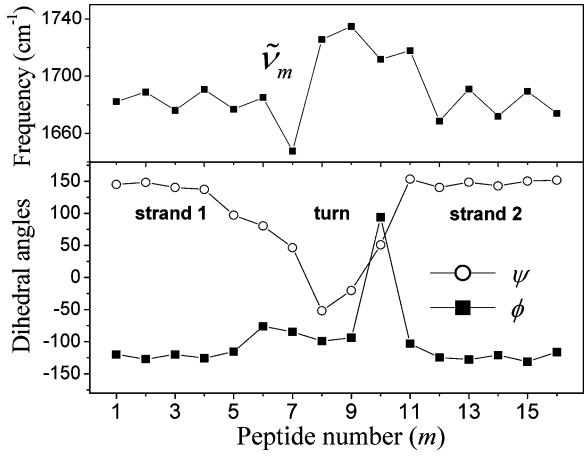

Figure 2. Local amide I mode frequencies of the A_{17} β hairpin obtained by using the Hessian matrix reconstruction method are plotted in the upper panel. The dihedral angles, ϕ_j and ψ_j, are plotted in the lower panel.

B. Local Mode Transition Dipoles and Couplings. Although in the previous studies,[32−34a] the transition dipole of each peptide group was assumed to be constant and to not depend on its position or on its local environment, the transition dipole of each amide I local mode can in fact vary due to the electronic structure changes induced by the local environment around each peptide bond. One can obtain the local mode transition dipoles separately as

$$\frac{\partial \mu}{\partial q_j} = \sum_m{}' U_{m,j} \frac{\partial \mu}{\partial r_m} \tag{2}$$

where μ, q_j, and r_m denote the dipole moment, the jth amide I local coordinate, and the mth mass-weighted atomic coordinate, respectively. Here, the prime over the summation means that the summation over m includes only the six atoms belonging to the jth peptide bond. In Figure 3a, $|\partial\mu/\partial q_j|$ and angle θ_j (see Figure 3a for the definition of θ) are plotted for the 17 amide I local oscillators. We find that the averages, $\langle|\partial\mu/\partial q_j|\rangle$ and $\langle\theta_j\rangle$, are 3.2 D Å^{-1} amu$^{-1/2}$ and 28°, and the corresponding standard deviations are 0.2 D Å^{-1} amu$^{-1/2}$ and 4°. Therefore, the approximation that the local mode transition dipoles do not depend strongly on local configurations of neighboring peptides or on hydrogen-bonding interactions is quantitatively acceptable. This observation is quite critical because the above approximation greatly simplifies the various numerical simulations of the linear and nonlinear spectra of proteins.

In Figure 3b, only the vibrational coupling constants, $j_{j,k}$, that are larger than 1 cm^{-1} are shown. The vibrational coupling strength between the two nearest neighboring peptides is relatively small, but that between two hydrogen-bonded peptides belonging to two different strands, for example, $\beta_{2,16}$, is comparatively large, about −6 cm^{-1}. The "X" shape of the coupling constant matrix in Figure 3b is a typical pattern found in the antiparallel β-sheet polypeptides.

III. Molecular Dynamics Simulation Results

In Section II, we considered the isolated A_{17} β hairpin. However, when it is dissolved in liquid water (D_2O), the local mode frequencies and vibrational coupling constants can fluctuate in time due to the peptide−water interactions and conformational fluctuation. If one carries out a molecular dynamics simulation of the aqueous A_{17} β-hairpin solution by using the force fields in the AMBER[35] program, for example, its structure will undergo a series of structural transitions and will eventually end up being a conformation that is completely different from that of the β hairpin. Therefore, we modified the intramolecular potential function in the AMBER program to make the polypeptide structure remain the same. Consequently, we lose information on the conformational fluctuation-induced vibrational-frequency shift and coupling-constant changes during the simulation run. Although this rigid solute simulation appears to be unrealistic, we have already found that the fluctuation amplitudes of the coupling constants due to polypeptide conformational fluctuations are very small and that the amide I local mode frequency fluctuations are dominated by the peptide−water interactions.[31,34a] As demonstrated in ref 31, the rigid polypeptide simulation provides both qualitatively and quantitatively acceptable results on the IR absorption, vibrational circular dichroism, and even 2D IR photon echo spectra of either unlabeled or isotope-labeled α-helical polypeptides in liquid water.

Second, we carry out a full MD simulation of the GB1 β-hairpin solution, in which all of the intramolecular degrees of freedom are allowed to move. Unlike the case of the A_{17} β hairpin, the overall structure of the GB1 β hairpin remains to be the stable hairpin throughout the simulation trajectory.

A. MD Simulation Methods. Molecular dynamics (MD) simulations were performed by using the SANDER module of the AMBER program package employing a parm99 force field[35] at constant temperature and pressure conditions. The A_{17} β-hairpin and the GB1 β-hairpin solutions at pH = 7 contain 4067 and 2164 TIP3P water molecules, respectively. In the case of the ideal A_{17} β-hairpin simulation, only the backbone dihedral rotations along the ϕ's and ψ's are constrained to make the backbone conformation rigid. However, such constraints are not implemented in the GB1 β-hairpin simulation. Long-range electrostatic interactions are treated with the particle-mesh Ewald method implemented in the AMBER program.[36] The solvated system was subject to 1000 steps of conjugate gradient energy minimization and then brought into an equilibrium state for 1 ns at 298 K using the Berendsen coupling algorithm for maintaining constant temperature and pressure.[37] During the simulation, an 8.0-Å nonbonded interaction cutoff was used. The system was then coupled to an external heat bath with a relaxation time of 1.2 ps. A 1-fs time step was used. Configuration data were saved every 10 (50) fs during the 2 ns simulation for the purpose of calculating IR spectra and hydrogen-bonding population analyses for the A_{17} (GB1) β hairpin.

B. Local Mode Frequency Fluctuation. The solvation-induced amide I mode frequency shift and fluctuation can be simulated by using the following formula developed recently

$$\delta\tilde{\nu}_m^{\text{water}}(t) = \sum_{j=1}^{4} l_j \phi_{j(m)}^{\text{water}}(t) \tag{3}$$

where the four parameters, l_j, are $l_O = -5.54 \times 10^{-3}$, $l_C = 1.60 \times 10^{-3}$, $l_N = 4.79 \times 10^{-3}$, and $l_H = -8.60 \times 10^{-4}$. Here, the dimension of l_j is a fraction of electronic charge, *e*. $\phi_{j(m)}^{\text{water}}$ is the electrostatic (Coulomb) potential created by the partial charges of the surrounding water molecules at the jth site of the mth peptide bond. The validity of the above method using eq 3 has been tested quantitatively for various NMA−water clusters,[38] aqueous NMA solution,[39,40] and NMA dissolved in liquid methanol[41] by making direct comparisons of numerically simulated amide I IR absorption and 2D IR spectra with experiments.[42−44] Therefore, the fluctuating amide I local mode

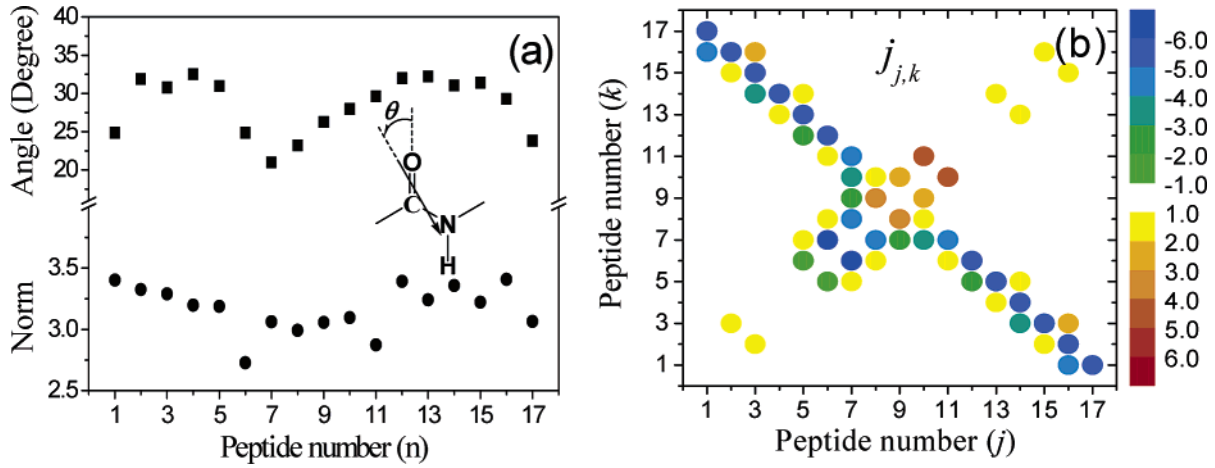

Figure 3. (a) Directions (θ angles) and absolute magnitudes of the local mode transition dipoles (in D Å^{-1} amu$^{-1/2}$) and (b) vibrational coupling constants of the A_{17} β hairpin, $j_{j,k}$ in cm^{-1}, are depicted.

frequency for the model A_{17} system at a given time, t, is given as

$$\tilde{\nu}_m(t) = \tilde{\nu}_m + \delta\tilde{\nu}_m^{\text{water}}(t) \quad (4)$$

where $\tilde{\nu}_m$ denotes the mth amide I local mode frequency (see Figure 2) obtained from the semiempirical quantum chemistry calculation of the gas-phase A_{17} β hairpin.

Although, in the case of the A_{17} β hairpin, the backbone structural fluctuation was not allowed, the effects from the conformational fluctuations and the interactions of peptide groups with other peptides and side chains should not be ignored for the simulation of the GB1 β hairpin. Recently, we developed a computational method for calculating those effects.[34] Frequency shifts induced by the other backbone peptides and side chain groups are estimated by using the following equations

$$\delta\tilde{\nu}_m^{\text{backbone}}(t) = \sum_{j=1}^{4} l_j \phi_{j(m)}^{\text{backbone}}(t)$$

and

$$\delta\tilde{\nu}_m^{\text{sidechain}}(t) = \sum_{j=1}^{4} l_j \phi_{j(m)}^{\text{sidechain}}(t)$$

where $\phi_{j(m)}^{\text{backbone}}$ and $\phi_{j(m)}^{\text{sidechain}}$ are the electrostatic potential from the partial charges of the other backbone peptide bonds and side-chain atoms, respectively. Here, we used the partial charge parameters of the backbone atoms given in ref 34 and those of the side-chain atoms given in the AMBER program, where the latter parameters were determined by using the restrained electrostatic potential (RESP) fit.[45] Thus, the amide I mode frequencies in the GB1 β hairpin is given by

$$\tilde{\nu}_m(t) = \tilde{\nu}^0 + \delta\tilde{\nu}_m^{\text{water}}(t) + \delta\tilde{\nu}_m^{\text{backbone}}(t) + \delta\tilde{\nu}_m^{\text{sidechain}}(t) \quad (5)$$

The reference frequency, which is that of the gas-phase NMA molecule, was denoted as $\tilde{\nu}^0$(equal to 1707 cm^{-1}).

In Figure 4a, the ensemble averaged amide I local mode frequencies, $<\tilde{\nu}_m>$, for $m = 1-17$, of the A_{17} β-hairpin solution are plotted (see the closed circles). Note that the $<\tilde{\nu}_m>$ values exhibit a zigzag pattern that is exactly opposite of that of the amide I local mode frequencies of the isolated A_{17} β hairpin. This comparison shows that the amide I local mode frequencies of the β hairpin in liquid water are dictated largely by the strong hydrogen-bonding interactions with the surrounding water molecules.

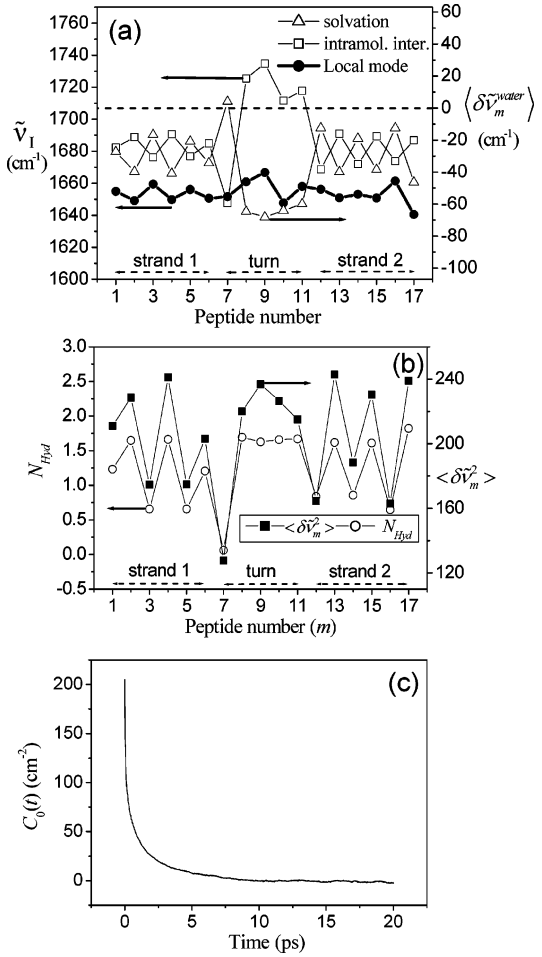

Figure 4. Molecular dynamics simulation results of the A_{17} β hairpin. (a) Ensemble averaged amide I local mode frequencies are shown as closed circles. Open squares are those obtained from the semiempirical quantum chemistry calculation results with the Hessian matrix reconstruction method, which are identical to the data shown in the upper panel of Figure 2. The open triangles are the ensemble averaged solvatochromic frequency shifts, that is, $\langle\delta\tilde{\nu}_m^{\text{water}}\rangle$. (b) The average number N_{Hyd} of hydrogen bonded water molecules around each carbonyl oxygen atom and the mean square fluctuation amplitude of amide I local mode frequencies are plotted. The frequency-frequency correlation function of the amide I local mode frequency, which was obtained by taking the average of all 17 correlation functions, is plotted in part c.

To estimate how large the local mode frequency fluctuations are and how strongly they depend on the position of each peptide

bond, we calculated the following mean square fluctuation amplitudes of the local mode frequencies for the A_{17} β-hairpin solution and plotted the results in Figure 4b

$$<\delta\tilde{\nu}_m{}^2> = <(\tilde{\nu}_m(t) - <\tilde{\nu}_m>)^2> \text{ for } m = 1-17 \quad (6)$$

where $<\delta\tilde{\nu}_m{}^2>$ varies from 120 to 240 cm^{-2}; note that the solvation reorganization energy associated with the vibrational transition is then in the range from 0.3 to 0.6 cm^{-1}. We found that the mean square frequency fluctuation amplitude is in good correlation with the number of solvating water molecules, N_{hyd}, that is, the average number of water molecules forming a direct hydrogen-bond with the carbonyl oxygen of the peptide groups (see the open circles in Figure 4b). Here, we assumed that the hydrogen bond is formed only when the distance between O(=C) and H(H_2O) is less than 3.3 Å and when the bond angle (OH−O) is between 135 and 225°. Now, to determine the time scale of the frequency−frequency correlation, we calculated all 17 time-correlation functions of the fluctuating local mode frequencies

$$C_m(t) = \langle\{\tilde{\nu}_m(t) - <\tilde{\nu}_m>\}\{\tilde{\nu}_m(0) - <\tilde{\nu}_m>\}\rangle \quad (7)$$

We found that, except for the initial values of $C_m(t)$, the correlation times and decaying patterns are very similar to one another. In Figure 4c, only the time correlation function averaged over the 17 different ones is plotted and it exhibits a typical bimodal decaying pattern. Although only the average correlation function, $C_0(t) = 17^{-1}\sum_m C_m(t)$, was presented in this paper, we use the entire 17 correlation functions, $C_m(t)$ for $m = 1-17$, in the numerical simulations of one- and two-dimensional IR spectra presented in Sections IV and V.

C. Instantaneous Normal Mode (INM) Analysis: A_{17} β Hairpin. In the following Section, IV, we will present a detailed discussion on how to calculate the IR absorption and 2D IR spectra by using the correlation function formalism. However, we find that the INM analysis can provide simple and instructive information on the delocalization, density of states, and vibrational phase correlations of various amide I normal modes. It begins with writing the amide I vibrational (one-exciton) Hamiltonian matrix as

$$H(t) = \begin{bmatrix} \tilde{\nu}_1(t) & j_{1,2} & j_{1,3} & \cdots & j_{1,N} \\ j_{1,2} & \tilde{\nu}_2(t) & j_{2,3} & \cdots & j_{2,N} \\ j_{1,3} & j_{2,3} & \tilde{\nu}_3(t) & \cdots & j_{3,N} \\ \vdots & \vdots & \vdots & \vdots & \vdots \\ j_{1,N} & j_{2,N} & j_{3,N} & \cdots & \tilde{\nu}_N(t) \end{bmatrix} \quad (8)$$

By performing a matrix diagonalization of the above Hamiltonian at time *t*, one can obtain the *instantaneous* amide I normal-mode frequencies and corresponding eigenvectors, that is, $V^T(t)\,H(t)\,V(t) = \Lambda(t)$. From the instantaneous configurations sampled from the MD trajectory, one can calculate the amide I INM spectrum (see Figure 5a), which is the *density of states (DOS) of the one-exciton band*

$$\rho(\omega) = \frac{1}{N}\langle\sum_\alpha \delta(\omega - \omega_\alpha)\rangle \quad (9)$$

Using the corresponding eigenvector elements obtained from each individual instantaneous configuration, we calculated the inverse participation ratio (IPR) that is a measure of the number of amide I local modes participating in a given normal mode.

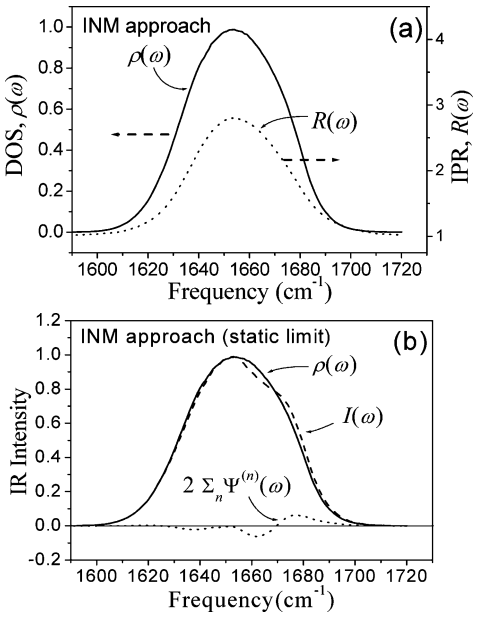

Figure 5. INM analysis results of the A_{17} β hairpin in liquid water. (a) The density of the one-exciton states, $\rho(\omega)$, and the inverse participation ratio, $R(\omega)$, are plotted. (b) The INM-calculated IR absorption spectrum, $I(\omega)$, is plotted as a dashed curve, and the average dipole strength-weighted density of the states and the second term in eq 14 are also plotted as solid and dotted curves, respectively.

Here, the IPR of the αth instantaneous normal mode, denoted as η_α, is defined as

$$\eta_\alpha \equiv (\sum_j V_{j,\alpha}^4)^{-1} \quad (10)$$

In Figure 5a, the calculated IPR spectrum defined as $R(\omega) \equiv N^{-1}\langle\sum_\alpha \eta_\alpha \delta(\omega - \omega_\alpha)\rangle/\rho(\omega)$ is also plotted together with $\rho(\omega)$. The magnitudes of the IPR values are relatively small, indicating that the instantaneous amide I normal modes are spatially delocalized on just a few local modes. The diagonal disorder induced by the peptide−water interaction and the existence of the turn region residues acting like an insulator prohibiting any through-bond coupling-induced delocalization are key factors making the INM less delocalized in space.

D. IR Absorption Spectrum in the Static Limit: INM Approach. Once the eigenvectors of the INMs are obtained, the transition dipole of the αth INM is given by a linear combination of the local mode transition dipoles as

$$\frac{\partial\mu}{\partial Q_\alpha} = \sum_n V_{n,\alpha}\frac{\partial\mu}{\partial q_n} \quad (11)$$

where Q_α is the αth amide I normal coordinate. The dipole strength of the αth INM can be written as

$$D_\alpha \equiv |\frac{\partial\mu}{\partial Q_\alpha}|^2 = \sum_n V_{n,\alpha}^2 |\frac{\partial\mu}{\partial q_n}|^2 + 2\sum_{n=1}^{N-1} P_\alpha{}^{(n)} \cong \left\langle\left|\frac{\partial\mu}{\partial q_n}\right|^2\right\rangle + 2\sum_{n=1}^{N-1} P_\alpha^{(n)} \quad (12)$$

where $\langle|\partial\mu/\partial q_n|^2\rangle$ is the average dipole strength of the amide I local mode and the auxiliary function, $P_\alpha^{(n)}$, is defined as

$$P_{\alpha}^{(n)} \equiv \sum_{i=1}^{N-n}\left(\frac{\partial\mu}{\partial q_i}\right)\cdot\left(\frac{\partial\mu}{\partial q_{i+n}}\right)V_{i,\alpha}V_{i+n,\alpha} \cong \left\langle\left|\frac{\partial\mu}{\partial q_i}\right|\right\rangle^2\sum_{i=1}^{2N-n}V_{i,\alpha}V_{i+n,\alpha}\cos\chi_{i,i+n} \quad (13)$$

Here, $\chi_{i,i+n}$ is the angle between the ith and $(i + n)$th local mode transition dipole vectors. The first term on the right-hand side of eq 12 does not depend on the backbone structure of a given polypeptide so that the characteristic IR band shapes of various polypeptides are determined mainly by the second term in eq 12. Note that the factor $P_{\alpha}^{(n)}$ carries information on the relative angles between two different peptide groups (local mode transition dipoles) as well as on their weights in the αth amide I normal mode.

In the INM picture, taking the ensemble averages of the dipole strength given in eq 12 weighted by the DOS, we have

$$I(\omega) = N^{-1}\langle\sum_{\alpha}D_{\alpha}\delta(\omega-\omega_{\alpha})\rangle \cong \langle|\partial\mu/\partial q_i|^2\rangle\rho(\omega) + 2\sum_{i=1}^{N-1}\Psi^{(i)}(\omega) \quad (14)$$

where

$$\Psi^{(n)}(\omega) \equiv N^{-1}\langle\sum_{\alpha}P_{\alpha}^{(n)}\delta(\omega-\omega_{\alpha})\rangle \quad (15)$$

Equation 14 shows that the INM-calculated IR absorption spectrum is given by a sum of two spectra. The first term is linearly proportional to DOS, $\rho(\omega)$. Although the peak position and shape of $\rho(\omega)$ are likely to be dependent on the 3D conformation of a given polypeptide, the overall shape of $\rho(\omega)$ does not depend strongly on the secondary structure. For instance, $\rho(\omega)$ of the α-helical polyalanine in liquid water was calculated recently (see Figure 4a of ref 34) and it appears to be quite similar to that of the β hairpin in liquid water considered in this paper. Therefore, the detailed line shape of the IR absorption band is critically determined by the second term in eq 14, which reflects the detailed polypeptide structures. To gain some more insight, let us consider $P_{\alpha}^{(1)}$, for example. From the definition in eq 13, $P_{\alpha}^{(1)}$ is a sum of weighted local mode transition dipole dot products. To understand the physical meaning of its value, let us consider the case of the α-helix. The angle $\chi_{i,i+1}$ between the two nearest-neighboring local mode transition dipole vectors is less than 90° so that we find $P_{\alpha}^{(1)} \propto \sum_{i=1}^{N-1}V_{i,\alpha}V_{i+1,\alpha}$. If the αth normal mode is *A*-mode-like, the signs of eigenvector elements are the same (in phase) and $P_{\alpha}^{(1)}$ is positive. Consequently, its contribution to the IR spectrum, $\Psi^{(1)}(\omega)$, will be positive, that is, adding more intensity to the absorption spectra at the frequency of the *A*-mode-like αth normal mode.[46] However, if the αth normal mode is *E*-mode-like, $\Psi^{(1)}(\omega)$ will negatively contribute to the spectrum. Similarly, one can understand the physical meanings of $P_{\alpha}^{(n)}$ and $\Psi^{(n)}(\omega)$.

In Figure 5b, we plot the two components in eq 14 separately and they are directly compared with the INM-calculated IR absorption spectrum (dashed line). Note that the band shape is highly asymmetric, which is a characteristic feature of the β hairpin experimentally observed by Arrondo et al. in ref 21. Although the INM analysis provides useful information on the absorption line shape, the width of the spectrum is broader than that of the experimental result. This can be understood by noting that the INM analysis corresponds to the limiting case when the line broadening is determined solely by the inhomogeneous (static) contribution. In other words, the motional narrowing process induced by the ultrafast relaxation of the frequency−frequency correlation function was not taken into account correctly in the numerical calculation of the absorption spectrum. Therefore, we will use the time-correlation function formalism to calculate not only the IR absorption spectrum but also the 2D IR spectrum in the following sections.

IV. IR Absorption Spectrum: Time-Correlation Function Approach

The IR absorption spectrum is given by the Fourier transform of the linear response function, $J(t)$

$$I(\omega) \approx \int_{-\infty}^{\infty}\mathrm{d}t\,\mathrm{e}^{i\omega t}J(t) \quad (16)$$

By using the semiclassical approximation discussed in ref 39, the linear response function, $J(t)$, can be written as

$$J(t) \cong \sum_{\alpha}D_{\alpha}\,\mathrm{e}^{-i\varpi_{\alpha}t}\langle\mathrm{e}^{-i\int_0^t\mathrm{d}\tau\,\delta\omega_{\alpha}(\tau)}\rangle \cong \sum_{\alpha}D_{\alpha}\,\mathrm{e}^{-i\varpi_{\alpha}t}\,\mathrm{e}^{-g_{\alpha}(t)}$$

$$g_{\alpha}(t) = \int_0^t\mathrm{d}\tau_1\int_0^{\tau_1}\mathrm{d}\tau_2\langle\delta\omega_{\alpha}(\tau_2)\delta\omega_{\alpha}(0)\rangle = \int_0^t\mathrm{d}\tau_1\int_0^{\tau_1}\mathrm{d}\tau_2\,C_{\alpha}(\tau_2) \quad (17)$$

where D_{α}, ϖ_{α}, and $\delta\omega_{\alpha}$ denote the dipole strength, the ensemble averaged normal-mode frequency, and the fluctuating part of the αth normal-mode frequency, respectively. To calculate the frequency−frequency correlation function, we divided the total Hamiltonian matrix into the ensemble (time) averaged and fluctuating parts, as $H(t) = H_0 + \delta H(t)$, and diagonalized the ensemble averaged (reference) Hamiltonian matrix, $W^{-1}H_0W = \Lambda$. Here, the off-diagonal elements of the $W^{-1}\delta H(t)W$ matrix are negligibly small so that the frequency−frequency correlation function of the αth normal mode can be written as

$$C_{\alpha}(t) = \langle\delta\omega_{\alpha}(t)\,\delta\omega_{\alpha}(0)\rangle \quad (18)$$

with

$$\delta\omega_{\alpha}(t) = \sum_{jk}W_{\alpha j}^{-1}\delta H_{jk}(t)\,W_{k\alpha} \quad (19)$$

If the off-diagonal matrix elements, $\delta H_{jk}(t)$ for $j\neq k$, are ignored, eq 19 simplifies to

$$\delta\omega_{\alpha}(t) = \sum_{j}\delta\Omega_j(t)\,W_{j\alpha}^2 \quad (20)$$

so that we have

$$C_{\alpha}(t) = \sum_{jk}W_{j\alpha}^2W_{k\alpha}^2\langle\delta\Omega_j(t)\,\delta\Omega_k(0)\rangle \quad (21)$$

where $\delta\Omega_k(t)$ (equal to $2\pi c\{\tilde{\nu}_k(t) - \langle\tilde{\nu}_k\rangle\}$) is the fluctuating angular frequency of the kth local mode. We found that $\langle\delta\Omega_j\delta\Omega_k\rangle$ for $j\neq k$ is about 1 order of magnitude smaller than the magnitude of the autocorrelation function, $\langle\delta\Omega_j^2\rangle$. Thus, one can further simplify eq 21 as

$$C_{\alpha}(t) = \sum_{j}W_{j\alpha}^4\langle\delta\Omega_j(t)\,\delta\Omega_j(0)\rangle \quad (22)$$

Invoking the final approximation that the time-correlation

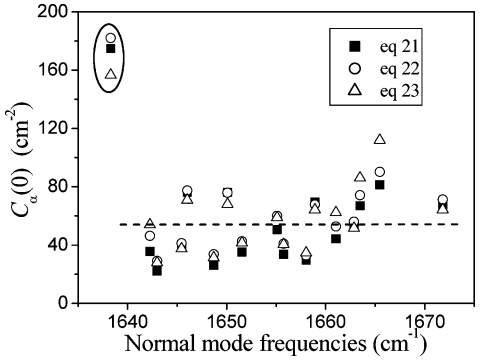

Figure 6. The mean square fluctuation amplitudes of 17 amide I normal-mode frequencies of the A_{17} β hairpin calculated by using eqs 21−23 are directly compared in this figure.

functions of the local mode frequency fluctuation are identical for all N local modes, we have

$$C_\alpha(t) = C_0(t)\sum_j W_{j\alpha}^4 = C_0(t)/\eta_\alpha \qquad (23)$$

where $C_0(t)$ is the average frequency−frequency correlation function of the amide I local mode (see Figure 4c). Note that the frequency−frequency correlation function of the αth normal mode can be significantly smaller than the local mode frequency−frequency correlation function by the factor of the inverse participation ratio, η_α. This phenomenon is known as the exchange narrowing process in the *J*-aggregate system. In Figure 6, the estimated mean square fluctuation amplitudes, $C_\alpha(0)$, obtained from eqs 21−23 for all 17 amide I *normal* modes are plotted as closed squares, open circles, and open triangles, respectively. It is found that the crudest approximate expression given in eq 23 is still quantitatively reliable, indicating that the series of approximations introduced above work well in the present case. In Figure 6, the lowest-frequency mode at 1638 cm^{-1} has the largest mean square fluctuation amplitude, that is, $C_1(0) > C_\alpha(0)$ (for all $\alpha = 2-17$). It turns out that this lowest-frequency normal mode is highly localized on the seventeenth peptide bond (see Figure 1), which does not form any intramolecular hydrogen bond with peptide 1 and is therefore exposed to the highly fluctuating electrostatic potential of the surrounding water molecules. Thus, its frequency fluctuation amplitude is comparatively larger than any other amide I normal modes. Other than this lowest-frequency normal mode, all of the other 16 normal modes are delocalized over a few peptide bonds so that the corresponding bands are significantly narrower than that of the highly localized normal mode 1.

A. IR Absorption Spectrum. Using eqs 16, 17, and 21, we numerically calculate the IR absorption spectra of the A_{17} and GB1 β hairpins and plot them in Figure 7a−c. The 17 Gaussian-like bands (thin solid lines) in Figure 7a correspond to each amide I normal mode absorption spectrum of the A_{17} β hairpin. In the upper panel of Figure 7a, the inverse participation ratios, η_α, are also shown so that one can easily verify that the more a given normal mode is delocalized the narrower the band shape is. In Figure 7b, the lifetime-broadened spectrum of A_{17} is plotted, where the lifetime broadening effect was taken into account in an ad hoc manner as

$$I(\omega) \approx \int_0^\infty \mathrm{d}t\, \mathrm{e}^{i\omega t} J(t)\, \mathrm{e}^{-\frac{t}{2T_1}} \qquad (24)$$

where T_1 denotes the average lifetime of the one-exciton state and is assumed to be 1 ps.

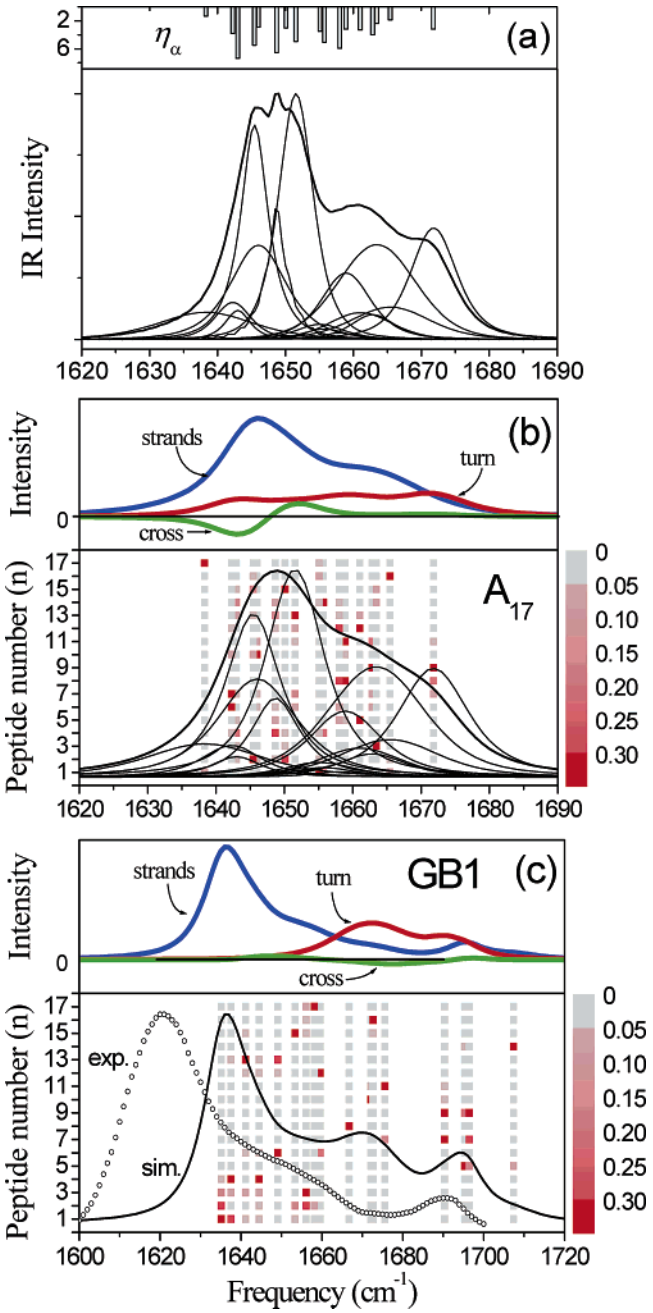

Figure 7. (a) Absorption line shapes (thin lines) of 17 normal mode transitions of the A_{17} β hairpin are plotted separately with the corresponding inverse participation ratios. (b) The IR absorption spectrum of the A_{17} β hairpin numerically calculated by using the time-correlation function formalism in eq 17 is plotted after approximately taking into account the lifetime broadening contribution. The blue, red, and green curves in the upper panel of the Figure 7b correspond to the three terms, $I_{strand}(\omega)$, $I_{turn}(\omega)$, and $I_{cross}(\omega)$, respectively. The color bars in the lower panel represent the squares of the eigenvector elements. (c) Absorption lines of the GB1 β hairpin are plotted. In the upper panel, three components of the spectrum, $I_{strand}(\omega)$, $I_{turn}(\omega)$, and $I_{cross}(\omega)$, are shown. The simulated absorption spectrum and the squares of eigenvector elements are plotted with the solid line and color bars in the lower panel. The experimentally measured absorption spectrum reported in ref 21 is also plotted (see the open circles).

Arrondo et al.[21] analyzed the IR spectrum of an aqueous β-hairpin solution by decomposing the amide I band with a few Gaussian functions and attempted to assign each component to specific amide I vibrations localized on particular positions in the β hairpin. Although such an analysis method has been found to be useful, quite often the mode assignments can be ambiguous

not only because of the delocalized natures of the amide I normal modes but also because of spectral congestion. However, in the present simulation study, it is possible to investigate which regions of the polypeptide residues contribute to which part of the absorption spectrum. One can divide the total transition dipole moment of the αth normal mode into two parts, that is, strand and turn contributions

$$\frac{\partial \mu}{\partial Q_\alpha} = \sum_{n\in\text{strand}} W_{n,\alpha}\frac{\partial \mu}{\partial q_n} + \sum_{n\in\text{turn}} W_{n,\alpha}\frac{\partial \mu}{\partial q_n} = \left(\frac{\partial \mu}{\partial Q_\alpha}\right)_{\text{strand}} + \left(\frac{\partial \mu}{\partial Q_\alpha}\right)_{\text{turn}} \quad (25)$$

The dipole strength is then given by a sum of three terms. Therefore, the absorption spectrum can be written as

$$I(\omega) = I_{\text{strand}}(\omega) + I_{\text{turn}}(\omega) + I_{\text{cross}}(\omega) \quad (26)$$

where the cross term, $I_{\text{cross}}(\omega)$, involves the dot products between a local mode transition dipole in the strand region and those in the turn region. In the upper panel of Figure 7b for the A_{17} β hairpin, the three components in eq 26 are plotted. Note that $I_{\text{strand}}(\omega)$ (see the blue curve) dictates the entire absorption spectrum and that the largest peak at 1643 cm^{-1} originates mainly from the local mode transition dipoles in the antiparallel β-sheet strand regions. The contributions from the local mode transition dipoles in the turn region (see the red curve in the upper panel of Figure 7b) are diffused, but the peak maximum of $I_{\text{turn}}(\omega)$ is at a high-frequency region around 1672 cm^{-1}. The cross spectrum, $I_{\text{cross}}(\omega)$, is relatively small compared to the geometric mean of $I_{\text{strand}}(\omega)$ and $I_{\text{turn}}(\omega)$, indicating that the mode mixing between turn-region local modes and strand-region local modes is comparatively small. In Figure 7b, the color bars show which normal modes are spatially delocalized on which peptide bonds. Apparently, the highest-frequency normal mode at 1672 cm^{-1} is highly localized on the local modes in the turn region (peptide numbers 7−9), whereas the low frequency normal modes are largely delocalized over the antiparallel β-sheet strand regions.

Although analyses of the A_{17} β-hairpin system give general information on the structure−spectrum relationship, in the real case of the GB1 β hairpin a number of complicating factors, for example, backbone structure fluctuation, the side-chain effect, and the conformational diversity of the side chains, influence the spectral line shape. In Figure 7c, we show the simulated IR spectrum of the GB1 β hairpin. Three peaks appear at 1636, 1670, and 1694 cm^{-1}. By comparing the spectra in the upper panel of Figure 7c to the total spectrum in the lower panel, it becomes clear that the peak at 1636 cm^{-1} is comprised mainly of the normal modes delocalized on the strands. The 1670 cm^{-1} peak can be attributed to the normal modes in the turn region, and the 1694 cm^{-1} peak is from both strands and turn. This peak assignment is surprisingly consistent with the mode assignments by Arrondo et al. and Hilario et al. in refs 21 and 47, where they used the factor analysis method. Also, the asymmetric line shape with a strong low-frequency peak, a weak high-frequency peak, and the existence of a shoulder in the middle is in good agreement with experiment; the open circles in Figure 7c are experimental data reproduced from ref 21.

B. Isotope-Labeling Effects. The isotope-labeling method has been used extensively because it provides a mean to overcome the spectral congestion problem. Here, we will specifically consider three different isotope-labeled β hairpins,

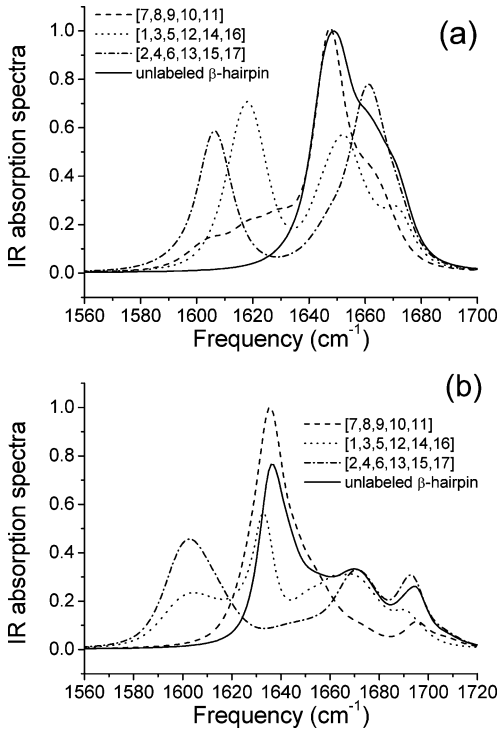

Figure 8. (a) The IR absorption spectra of the three isotope-labeled A_{17} β hairpins, [1,3,5,12,14,16], [2,4,6,13,15,17], and [7,8,9,10,11], are plotted as the dotted, dash-dotted, and dashed lines, respectively, and compared with that (solid line) of the unlabeled one. (b) Three isotope-labeled spectra of the GB1 β hairpin, [1,3,5,12,14,16], [2,4,6,13,15,-17], and [7,8,9,10,11], are plotted with dotted, dash-dotted, and dashed lines, respectively, and compared with that (solide line) of the unlabeled one.

denoted as [7,8,9,10,11], [1,3,5,12,14,16], and [2,4,6,13,15,17]. The numbers in the bracket correspond to the positions of the $^{13}C{=}^{16}O$ isotope-labeled peptide bonds (see Figure 1). In the case of [1,3,5,12,14,16], all six carbonyl groups of peptides 1, 3, 5, 12, 14, and 16 point inward to form intramolecular hydrogen bonds, whereas peptides 2, 4, 6, 13, 15, and 17 point outward and they are exposed to the surrounding water molecules forming strong hydrogen bonds. In Figure 8a, the simulated absorption spectra of the isotope-labeled A_{17} β hairpins are depicted and compared with those of the unlabeled one (solid line), and one can immediately find several notable isotope-labeling effects. For [1,3,5,12,14,16] and [2,4,6,13,15,-17], the isotope peaks are clearly frequency-resolved from the (unlabeled) main peak and they appear at 1618 and 1606 cm^{-1}, respectively. The reason that the two isotope peak frequencies of [1,3,5,12,14,16] and [2,4,6,13,15,17] differ from each other by about 12 cm^{-1} is because peptides 2, 4, 6, 13, 15, and 17 are exposed to solvent water molecules and thus are strongly red-shifted. Second, the isotope exchange in the case of [2,4,6,-13,15,17] induces a dramatic intensity decrease of the main peak of the unlabeled A_{17} β hairpin at 1650 cm^{-1} without strongly affecting the line shape in the high-frequency region (>1670 cm^{-1}). This result can be understood by noting that $I_{\text{strand}}(\omega)$ in the upper panel of Figure 7b has a strong peak at 1650 cm^{-1}. Thus, the isotope-labeling effect on the [2,4,6,13,15,17] spectrum is to reduce the IR intensities around 1650 cm^{-1}. The line shape and intensity distribution of the [1,3,5,12,14,16] spectrum in the frequency range from 1640 to 1680 cm^{-1} are even more strongly altered by the isotope labelings. This observation reveals that those peptides involved in the *intramolecular* hydrogen bonds strongly participate in the amide I normal modes carrying large oscillator strengths.

When the five residues in the turn region are isotope-labeled, that is, [7,8,9,10,11], the isotope peak is not frequency-resolved but rather appears as a broad and featureless shoulder contribution to the A_{17} β-hairpin spectrum in the frequency range from 1590 to 1640 cm^{-1}. This puzzling result turns out to be related to the fact that the local mode frequencies of peptides 7−11 are dispersed and the positively large vibrational coupling constants between them make the normal-mode frequencies of the isotope-labeled pentapeptides (7−8−9−10−11) distribute over a wide frequency range. Second, the isotope labeling at the turn region induces a significant reduction of the high frequency (>1655 cm^{-1}) shoulder peak of the unlabeled β hairpin. This pattern is again found to be consistent with the observation that $I_{turn}(\omega)$ of the A_{17} β hairpin peaks at around 1660−1680 cm^{-1} (see Figure 7b).

Also, we studied the same isotope-labeling effects on the real GB1 β-hairpin spectrum (Figure 8b). The general patterns are the same as those of the A_{17} β hairpin. Only when the isotope-labeled peptides are in the two strands, such as [1,3,5,12,14,-16] and [2,4,6,13,15,17], the isotope peak appears at ∼1600 cm^{-1} with a notable intensity lowering of the 1640 cm^{-1} peak. Similarly, one can understand why the IR intensity at ∼1640 cm^{-1} in the [7,8,9,10,11] spectrum increases upon isotope labeling.

V. Two-Dimensional Vibrational Spectra

By displaying the IR photon echo signal of a polypeptide in the 2D frequency space, one can achieve a significantly improved frequency resolution and obtain a great deal of information on the vibrational couplings and consequently its 3D structure.[48−51] Most of the previous works on numerically simulating 2D vibrational echo spectra, which have been presented by us and others, used the Markovian approximation[34a] to the line-shape functions. In the present work, we will use the time-correlation function formalism to simulate the 2D IR photon echo correlation spectra of A_{17} and GB1 β hairpins, both unlabeled and isotope-labeled ones.

A. Photon Echo Nonlinear Response Functions. By denoting the vibrational one- and two-exciton states as $|e_j>$ and $|f_k>$, we define the frequency−frequency correlation functions as

$$\xi_{e_ie_j}(\tau_1, \tau_2) \equiv \langle \delta\omega_{e_ig}(\tau_1)\delta\omega_{e_jg}(\tau_2)\rangle$$

In ref 48, for a general multilevel system the detailed expressions for various nonlinear response function components were presented. For the present case of the IR photon echo, the nonlinear response function components are given as

$$R^{(1)}_{e_je_i}(t_3, t_2, t_1) = \langle \mu_{e_ig}\mu_{ge_j}\mu_{e_jg}\mu_{ge_i}\rangle \exp\{i\omega_{ge_i}t_3 + i\omega_{e_je_i}t_2 - i\omega_{e_ig}t_1\} \times \exp\{-\int_{t_1}^{t_1+t_2} d\tau_1 \int_{t_1}^{\tau_1} d\tau_2\, \xi^*_{e_je_j}(\tau_1, \tau_2) - \int_0^{t_1+t_2+t_3} d\tau_1 \int_0^{\tau_1} d\tau_2\, \xi_{e_ie_i}(\tau_1, \tau_2) + \int_{t_1}^{t_1+t_2} d\tau_1 \int_0^{t_1+t_2+t_3} d\tau_2\, \xi_{e_je_i}(\tau_1, \tau_2)\}$$

$$R^{(2)}_{e_je_i}(t_3, t_2, t_1) = \langle \mu_{ge_j}\mu_{e_ig}\mu_{e_jg}\mu_{ge_i}\rangle \exp\{i\omega_{ge_i}t_3 + i\omega_{e_je_i}t_2 + i\omega_{e_jg}t_1\} \times \exp\{-\int_0^{t_1+t_2} d\tau_1 \int_0^{\tau_1} d\tau_2\, \xi^*_{e_je_j}(\tau_1, \tau_2) - \int_{t_1}^{t_1+t_2+t_3} d\tau_1 \int_{t_1}^{\tau_1} d\tau_2\, \xi_{e_ie_i}(\tau_1, \tau_2) + \int_0^{t_1+t_2} d\tau_1 \int_{t_1}^{t_1+t_2+t_3} d\tau_2\, \xi_{e_je_i}(\tau_1, \tau_2)\}$$

$$R^{(3)}_{e_je_i}(t_3, t_2, t_1) = \langle \mu_{ge_j}\mu_{e_jg}\mu_{e_ig}\mu_{ge_i}\rangle \exp\{i\omega_{ge_i}t_3 + i\omega_{e_jg}t_1\} \times \exp\{-\int_0^{t_1} d\tau_1 \int_0^{\tau_1} d\tau_2\, \xi^*_{e_je_j}(\tau_1, \tau_2) - \int_{t_1+t_2}^{t_1+t_2+t_3} d\tau_1 \int_{t_1+t_2}^{\tau_1} d\tau_2\, \xi_{e_ie_i}(\tau_1, \tau_2) + \int_0^{t_1} d\tau_1 \int_{t_1+t_2}^{t_1+t_2+t_3} d\tau_2\, \xi_{e_je_i}(\tau_1, \tau_2)\}$$

$$R^{(4)}_{e_je_i}(t_3, t_2, t_1) = \langle \mu_{e_ig}\mu_{ge_j}\mu_{e_jg}\mu_{ge_i}\rangle \exp\{-i\omega_{e_jg}t_3 - i\omega_{e_ig}t_1\} \times \exp\{-\int_{t_1+t_2}^{t_1+t_2+t_3} d\tau_1 \int_{t_1+t_2}^{\tau_1} d\tau_2\, \xi_{e_je_j}(\tau_1, \tau_2) - \int_0^{t_1} d\tau_1 \int_0^{\tau_1} d\tau_2\, \xi_{e_ie_i}(\tau_1, \tau_2) - \int_{t_1+t_2}^{t_1+t_2+t_3} d\tau_1 \int_0^{t_1} d\tau_2\, \xi_{e_je_i}(\tau_1, \tau_2)\}$$

$$R^{(5)}_{f_ke_je_i}(t_3, t_2, t_1) = -\langle \mu_{ge_j}\mu_{e_jg}\mu_{f_ke_j}\mu_{e_jf_k}\rangle \exp\{-i\omega_{f_ke_j}t_3 - i\omega_{e_je_i}t_2 + i\omega_{e_ig}t_1\} \times \exp\{-\int_{t_1}^{t_1+t_2} d\tau_1 \int_{t_1}^{\tau_1} d\tau_2\, \xi_{e_je_j}(\tau_1, \tau_2) - \int_{t_1+t_2}^{t_1+t_2+t_3} d\tau_1 \int_{t_1+t_2}^{\tau_1} d\tau_2\, \xi_{f_kf_k}(\tau_1, \tau_2) - \int_0^{t_1+t_2+t_3} d\tau_1 \int_0^{\tau_1} d\tau_2\, \xi^*_{e_ie_i}(\tau_1, \tau_2) - \int_{t_1}^{t_1+t_2} d\tau_1 \int_{t_1+t_2}^{t_1+t_2+t_3} d\tau_2\, \xi^*_{e_jf_k}(\tau_1, \tau_2) + \int_{t_1}^{t_1+t_2} d\tau_1 \int_0^{t_1+t_2+t_3} d\tau_2\, \xi^*_{e_je_i}(\tau_1, \tau_2) + \int_{t_1+t_2}^{t_1+t_2+t_3} d\tau_1 \int_0^{t_1+t_2+t_3} d\tau_2\, \xi^*_{f_ke_i}(\tau_1, \tau_2)\}$$

$$R^{(6)}_{f_ke_je_i}(t_3, t_2, t_1) = -\langle \mu_{e_jg}\mu_{ge_j}\mu_{f_ke_j}\mu_{e_jf_k}\rangle \exp\{-i\omega_{f_ke_i}t_3 - i\omega_{e_je_i}t_2 - i\omega_{e_jg}t_1\} \times \exp\{-\int_0^{t_1+t_2} d\tau_1 \int_0^{\tau_1} d\tau_2\, \xi_{e_je_j}(\tau_1, \tau_2) - \int_{t_1+t_2}^{t_1+t_2+t_3} d\tau_1 \int_{t_1+t_2}^{\tau_1} d\tau_2\, \xi_{f_kf_k}(\tau_1, \tau_2) - \int_{t_1}^{t_1+t_2+t_3} d\tau_1 \int_{t_1}^{\tau_1} d\tau_2\, \xi^*_{e_ie_i}(\tau_1, \tau_2) - \int_0^{t_1+t_2} d\tau_1 \int_{t_1+t_2}^{t_1+t_2+t_3} d\tau_2\, \xi^*_{e_jf_k}(\tau_1, \tau_2) + \int_0^{t_1+t_2} d\tau_1 \int_{t_1}^{t_1+t_2+t_3} d\tau_2\, \xi^*_{e_je_i}(\tau_1, \tau_2) + \int_{t_1+t_2}^{t_1+t_2+t_3} d\tau_1 \int_{t_1}^{t_1+t_2+t_3} d\tau_2\, \xi^*_{f_ke_i}(\tau_1, \tau_2)\}$$

$$R^{(7)}_{f_ke_je_i}(t_3, t_2, t_1) = -\langle \mu_{e_jg}\mu_{f_ke_j}\mu_{ge_j}\mu_{e_jf_k}\rangle \exp\{-i\omega_{f_ke_i}t_3 - i\omega_{f_kg}t_2 - i\omega_{e_jg}t_1\} \times \exp\{-\int_0^{t_1} d\tau_1 \int_0^{\tau_1} d\tau_2\, \xi_{e_je_j}(\tau_1, \tau_2) - \int_{t_1}^{t_1+t_2+t_3} d\tau_1 \int_{t_1}^{\tau_1} d\tau_2\, \xi_{f_kf_k}(\tau_1, \tau_2) - \int_{t_1+t_2}^{t_1+t_2+t_3} d\tau_1 \int_{t_1+t_2}^{\tau_1} d\tau_2\, \xi^*_{e_ie_i}(\tau_1, \tau_2) - \int_0^{t_1} d\tau_1 \int_{t_1}^{t_1+t_2+t_3} d\tau_2\, \xi^*_{e_jf_k}(\tau_1, \tau_2) + \int_0^{t_1} d\tau_1 \int_{t_1+t_2}^{t_1+t_2+t_3} d\tau_2\, \xi^*_{e_je_i}(\tau_1, \tau_2) + \int_{t_1}^{t_1+t_2+t_3} d\tau_1 \int_{t_1+t_2}^{t_1+t_2+t_3} d\tau_2\, \xi^*_{f_ke_i}(\tau_1, \tau_2)\}$$

$$R^{(8)}_{f_ke_je_i}(t_3, t_2, t_1) = \langle \mu_{e_jg}\mu_{f_ke_j}\mu_{e_jf_k}\mu_{ge_j}\rangle \exp\{-i\omega_{e_jg}t_3 - i\omega_{f_kg}t_2 - i\omega_{e_jg}t_1\} \times \exp\{-\int_{t_1+t_2}^{t_1+t_2+t_3} d\tau_1 \int_{t_1+t_2}^{\tau_1} d\tau_2\, \xi_{e_je_j}(\tau_1, \tau_2) - \int_{t_1}^{t_1+t_2} d\tau_1 \int_{t_1}^{\tau_1} d\tau_2\, \xi_{f_kf_k}(\tau_1, \tau_2) - \int_0^{t_1} d\tau_1 \int_0^{\tau_1} d\tau_2\, \xi_{e_ie_i}(\tau_1, \tau_2) - \int_{t_1+t_2}^{t_1+t_2+t_3} d\tau_1 \int_{t_1}^{t_1+t_2} d\tau_2\, \xi_{e_jf_k}(\tau_1, \tau_2) - \int_{t_1+t_2}^{t_1+t_2+t_3} d\tau_1 \int_0^{t_1} d\tau_2\, \xi_{e_je_i}(\tau_1, \tau_2) - \int_{t_1}^{t_1+t_2} d\tau_1 \int_0^{t_1} d\tau_2\, \xi_{f_ke_i}(\tau_1, \tau_2)\} \quad (27)$$

where $\langle\mu\mu\mu\mu\rangle$ denotes the orientation average. The total nonlinear response function is given by a sum of all eight components in eq 27, where the summations of all of the one- and two-exciton states should be performed. To construct the two-exciton Hamiltonian of the β hairpin, the overtone and combination mode anharmonicities of each amide I local mode are assumed to be 16 and 1 cm^{-1}, respectively; note that in the case of perfect harmonic oscillators, the nonlinear transition pathways producing cross peaks exactly cancel out with one other. The ensemble averaged two-exciton Hamiltonian is first obtained and diagonalized to find two-exciton state energies and eigenvectors. Then, the frequency fluctuations of all of the two-exciton states are calculated by using eq 19 to evaluate the time-correlation functions, such as $\xi_{f_kf_k}(\tau_1, \tau_2)$, $\xi_{e_ie_j}(\tau_1, \tau_2)$, and $\xi_{e_jf_k}(\tau_1, \tau_2)$. Once the time-domain nonlinear response functions in eq 27 are obtained, their 2D Fourier transforms with respect to t_1 and t_3 variables are directly related to the 2D photon echo spectra. Depending on the detailed time-evolution processes of different nonlinear optical transition pathways, the 2D spectral components can be divided into the rephasing and nonrephasing contributions, that is[52]

$$S_R(\tilde{\nu}_3, \tilde{\nu}_1) = R^{(2)}(\tilde{\nu}_3, \tilde{\nu}_1) + R^{(3)}(\tilde{\nu}_3,\tilde{\nu}_1) + R^{(5)}(\tilde{\nu}_3,\tilde{\nu}_1)$$

$$S_{NR}(\tilde{\nu}_3, \tilde{\nu}_1) = R^{(1)}(\tilde{\nu}_3,\tilde{\nu}_1) + R^{(4)}(\tilde{\nu}_3, \tilde{\nu}_1) + R^{(6)}(\tilde{\nu}_3,\tilde{\nu}_1) + R^{(7)}(\tilde{\nu}_3, \tilde{\nu}_1) + R^{(8)}(\tilde{\nu}_3,\tilde{\nu}_1)$$

$$S_C(\tilde{\nu}_3, \tilde{\nu}_1) \equiv S_R(\tilde{\nu}_3, \tilde{\nu}_1) + S_{NR}(\tilde{\nu}_3, \tilde{\nu}_1) \quad (28)$$

where S_C is the so-called 2D correlation spectrum. The two frequencies, $\tilde{\nu}_1$ and $\tilde{\nu}_3$, are the conjugate Fourier frequencies associated with t_1 and t_3, respectively. Note that we have correctly taken into account the delocalization effect, the correlations of excitation frequency and probing frequency, the exchange narrowing processes, and all of the cross-correlations between two different one- or two-exciton state frequency fluctuations in the present calculation, which could not be quantitatively included in the previous Markovian approximation method. Finally, the lifetime broadening contribution to the nonlinear response functions were taken into account in an ad hoc manner. Assuming that the one- and two-exciton states have different lifetime broadening factors, γ_1 and γ_2, respectively, we multiply the following lifetime broadening functions to the vibrational nonlinear response functions in eq 27

$$\Gamma_1(t_3, t_2, t_1) = \exp\left\{-\frac{\gamma_1 t_3}{2} - \gamma_1 t_2 - \frac{\gamma_1 t_1}{2}\right\}$$

$$\Gamma_2(t_3, t_2, t_1) = \exp\left\{-\frac{(\gamma_1+\gamma_2) t_3}{2} - \gamma_1 t_2 - \frac{\gamma_1 t_1}{2}\right\}$$

$$\Gamma_3(t_3, t_2, t_1) = \exp\left\{-\frac{(\gamma_1+\gamma_2) t_3}{2} - \frac{(\gamma_1+\gamma_2) t_2}{2} - \frac{\gamma_1 t_1}{2}\right\} \quad (29)$$

where Γ_1, Γ_2, and Γ_3 are to be multiplied to $R^{(n)}$ of $n = 1-4$, those of $n = 5$ and 6, and those of $n = 7$ and 8, respectively. In the present simulation, the two parameters, γ_1 and γ_2, are assumed to be 1 and 2 ps^{-1}, respectively.

B. 2D IR Correlation Spectra of the A_{17} β Hairpin. The 2D IR correlation spectrum of the (unlabeled) A_{17} β hairpin is shown in Figure 9a. One can identify two diagonal peaks that were not clearly frequency-resolved in the corresponding IR absorption spectrum (see the solid line in Figure 8a). Furthermore, the cross-peak is also visible, though its amplitude is relatively small. The 2D contour line shape resembles that of an antiparallel β-sheet polypeptide, that is, the Z-shaped pattern that was first observed by Tokmakoff and co-workers.[25]

In Section IV, we separately considered contributions from the peptides in the two strands and turn regions to the IR absorption spectrum. Deliberately nullifying the local mode transition dipoles of peptides in either the strand or turn region, one can obtain two different 2D IR correlation spectra, $S_C^{strand}(\tilde{\nu}_3, \tilde{\nu}_1)$ and $S_C^{turn}(\tilde{\nu}_3, \tilde{\nu}_1)$, which are plotted in Figure 9b and c, respectively. Scaling the maximum peak intensity of $S_C(\tilde{\nu}_3, \tilde{\nu}_1)$ in Figure 9a, one can directly compare the relative peak amplitudes in $S_C^{strand}(\tilde{\nu}_3, \tilde{\nu}_1)$ and $S_C^{turn}(\tilde{\nu}_3, \tilde{\nu}_1)$ with those of the total spectrum, $S_C(\tilde{\nu}_3, \tilde{\nu}_1)$. It turns out that the entire 2D correlation spectrum is determined by $S_C^{strand}(\tilde{\nu}_3, \tilde{\nu}_1)$, indicating that the contributions from the peptides in the turn region are negligibly small. Because the absolute magnitude of each peak in the 2D IR spectrum is determined by the fourth power of the transition dipoles, the relative magnitudes of peaks in $S_C^{turn}(\tilde{\nu}_3, \tilde{\nu}_1)$ is much smaller than those in $S_C^{strand}(\tilde{\nu}_3, \tilde{\nu}_1)$; note that the dipole strengths (absolute square of normal mode transition dipole) contributed from the peptides in the turn region is about one-third of those in the strand region (see the figure in the upper panel of Figure 7b).

To further study the local structure dependencies of the 2D IR spectrum, we considered the three isotopomers, [1,3,5,12,-14,16], [2,4,6,13,15,17], and [7,8,9,10,11]. Their 2D spectra depicted in Figure 9d−f, respectively, are found to be dependent strongly on the isotope-labeling patterns. From these 2D spectra, we found a number of interesting features that can be understood by considering both the intra- or intermolecular hydrogen bonding interactions and the nature of the delocalized amide I vibrations. In the case when peptides 1, 3, 5, 12, 14, and 16 are $^{13}C{=}O$ labeled, in addition to the two frequency-resolved diagonal peaks already observed in the 2D spectra of the unlabeled β hairpin in Figure 9a, an isotope peak at 1619 cm^{-1} can be identified and its intensity is found to be even larger than those of the other two diagonal peaks at 1653 and 1673 cm^{-1}. Note that the latter two diagonal peaks are associated with amide I normal modes delocalized on peptides 2, 4, 6, 13, 15, and 17. Consequently, the absolute magnitudes of the transition dipoles associated with the amide I normal modes delocalized on peptides 2, 4, 6, 13, 15, and 17 are weaker than those on 1, 3, 5, 12, 14, and 16. This result is consistent with the intensity distribution of the two peaks in the IR absorption spectra of [1,3,5,12,14,16] and [2,4,6,13,15,17] in Figure 8a. In Figure 9d, one can also find the two strong cross peaks, A and B, in the upper-left region, which are clear evidence that the isotope-labeled amide I normal modes are strongly coupled to the unlabeled amide I normal modes. To understand the origin of these strong cross peaks, one should examine the coupling constant matrix shown in Figure 3b. It is noted that the coupling constants between the two nearest neighboring peptides in the strand are relatively small (see Figure 3b). However, coupling constants $j_{1,17}$, $j_{2,16}$, $j_{3,15}$, $j_{4,14}$, $j_{5,13}$, and $j_{6,12}$ are negatively large (~ -6 cm^{-1}). Therefore, any given amide I normal modes delocalized on peptides 1, 3, 5, 12, 14, and 16 can be coupled to those on peptides 2, 4, 6, 13, 15, 17 due to the hydrogen bond-induced vibrational interactions.

In Figure 9e, the 2D IR spectrum of [2,4,6,13,15,17] is plotted. The frequency of the diagonal isotope peak is again 12 cm^{-1} red-shifted in comparison to that of [1,3,5,12,14,16] shown in Figure 9d. Another interesting feature is that there is only

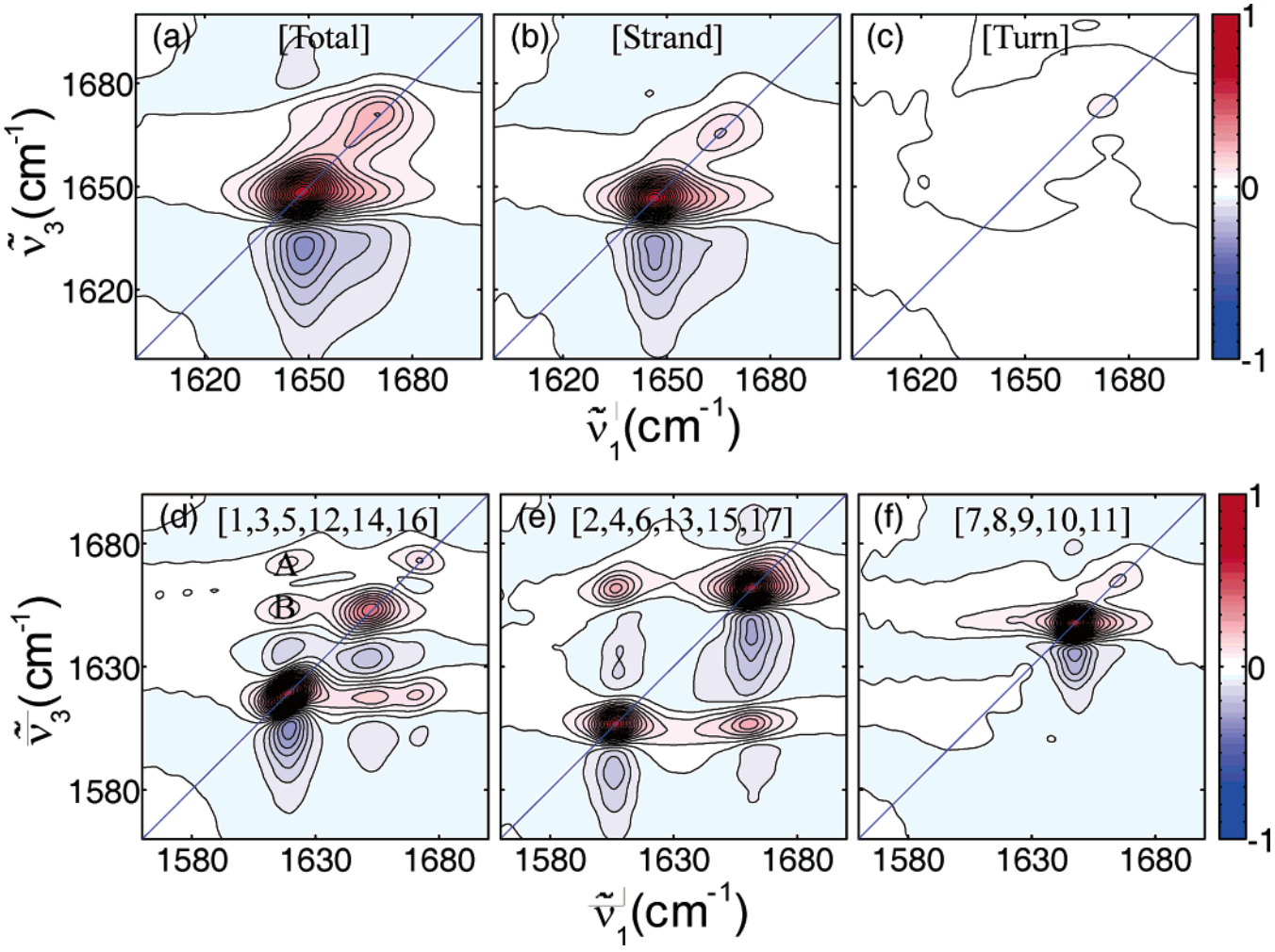

Figure 9. The parallel polarization ZZZZ-components of the 2D IR correlation spectra of the A_{17} β hairpin. (a) Two-dimensional IR photon echo spectrum of the unlabeled β hairpin is shown in this figure. The second (b) and third (c) spectra correspond to the cases in which either the local mode transition dipoles in the turn region or those in the strand regions are assumed to be zero, respectively. The absolute *z*-axis scales of the three figures (a−c) are the same so that one can quantitatively compare them. Two-dimensional IR photon echo spectra of [1,3,5,12,14,16], [2,4,6,13,15,17], and [7,8,9,10,11], are plotted in figures d−f, respectively.

one diagonal (unlabeled) peak at 1662 cm^{-1}. Also, there is a single cross peak at ($\tilde{\nu}_1$ = 1607 cm^{-1} and $\tilde{\nu}_3$ = 1662 cm^{-1}).

Let us consider the case of [7,8,9,10,11], in which all five of the peptide bonds in the turn region are isotope-labeled (Figure 9f). First of all, no isotope peaks appear along the diagonal line. Second, the entire 2D IR spectrum is close to that of the unlabeled β hairpin in Figure 9a. However, the major (strongest) diagonal peak is significantly elongated along the $\tilde{\nu}_1$ and $\tilde{\nu}_3$ axes. The latter observation suggests that the amide I normal modes delocalized on the two strands are to some extent coupled to the isotope-labeled amide I normal modes localized in the turn region. This result can be justified by the large coupling constant, $j_{6,7}$ (equal to $j_{7,6}$).

C. 2D IR Correlation Spectra of the GB1 β Hairpin. The 2D correlation spectra of the GB1 β hairpin are shown in Figure 10. From Figure 10a−c, it is found that the high-frequency diagonal peaks at 1670 and 1694 cm^{-1} originate from the amide I normal modes delocalized in the turn region. However, the lowest frequency diagonal peak at 1638 cm^{-1} is associated with those in the strand region.

The 2D IR spectrum of [1,3,5,12,14,16] exhibits four diagonal peaks at 1602, 1633, 1673, and 1691 cm^{-1} and multiple cross peaks. However, the 2D IR spectrum of [2,4,6,13,15,17] in Figure 10e is fairly different from that of [1,3,5,12,14,16] in Figure 10d. The diagonal peak at 1638 cm^{-1} in Figure 10a almost disappears in Figure 10e because of the isotope-exchange-induced frequency shifts of the ∼1638 cm^{-1} normal modes. However, the cross peaks between the isotope band and the high-frequency bands (at 1670 and 1694 cm^{-1}) are still clearly observed.

Finally, if the five peptides in the turn region of the GB1 β hairpin are isotope-labeled, then the characteristic 2D spectral features in Figure 10a are largely destroyed and only one strong diagonal peak at 1640 cm^{-1} appears in the spectrum, Figure 10f.

The realistic GB1 β hairpin is a far more complicated system in comparison to the A_{17} β hairpin because (1) the 3D backbone and side chain conformations fluctuate in solution, (2) the interpeptide coupling constants and local mode frequencies are thus stochastically varying in time, and (3) the polar and nonpolar amino acid side chains interact with the backbone peptides. However, the general shapes of the IR and 2D IR spectra of the GB1 β hairpin are quite similar to those of the A_{17} β hairpin. This observation suggests that the 1D and 2D spectral line shapes are determined largely by the global secondary structure and hydrogen-bonding pattern.

VI. Summary

By carrying out semiempirical quantum chemistry calculations and molecular dynamics simulations, we have theoretically

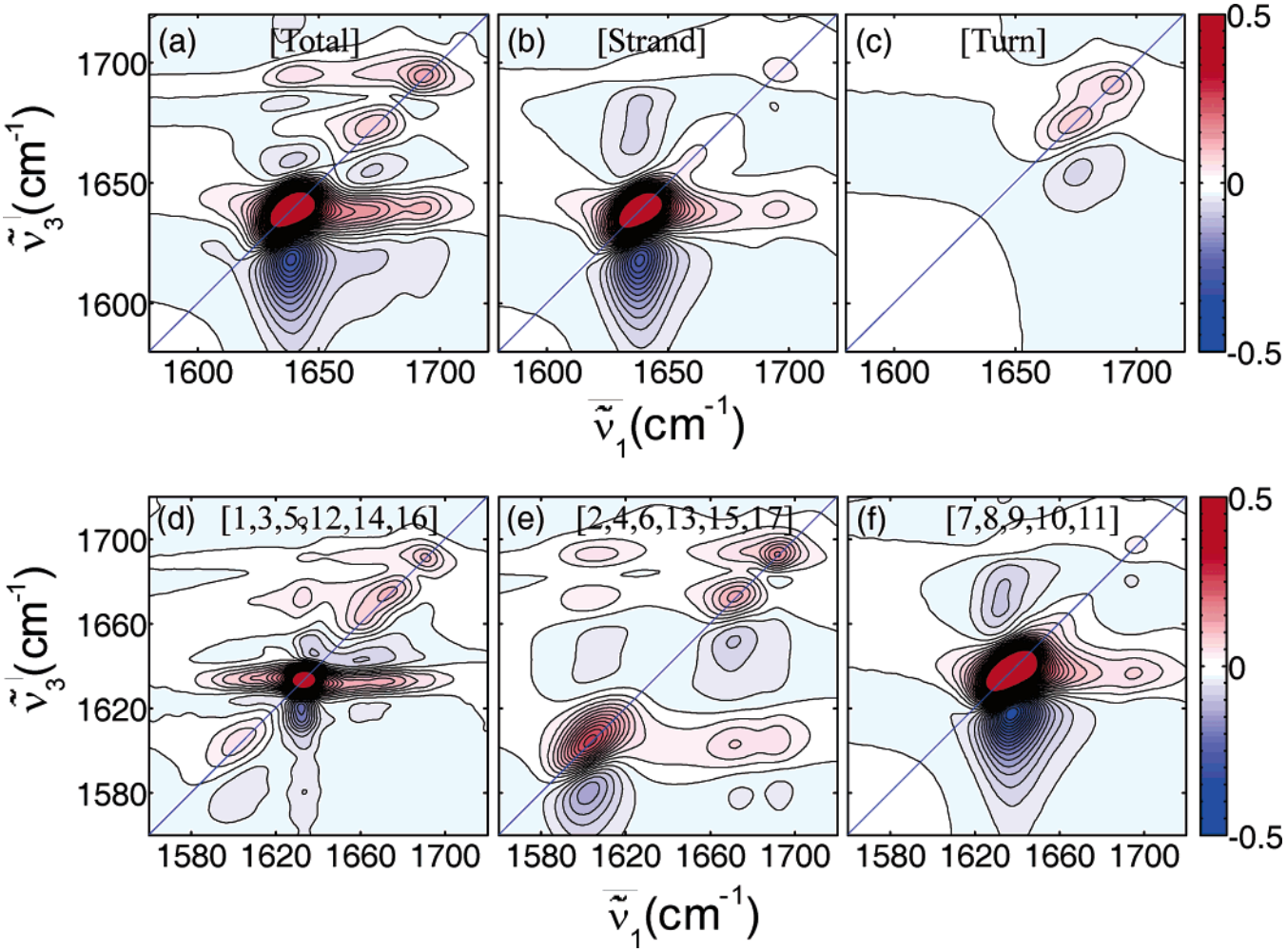

Figure 10. The 2D IR correlation spectra of the GB1 β hairpin. (a) Two-dimensional IR photon echo spectrum of the unlabeled β hairpin is shown in this figure. The second (b) and third (c) spectra correspond to the cases in which either the local mode transition dipoles in the turn region or those in the strand regions are assumed to be zero, respectively. The 2D IR photon echo spectra of [1,3,5,12,14,16], [2,4,6,13,15,17], and [7,8,9,-10,11], are plotted in figures d−f, respectively, in which each spectra is normalized with a maximum intensity of the unlabeled β-hairpin spectrum. The absolute *z*-axis scales of all six figures (a−f) are the same.

studied the vibrational properties and characteristic features of the alanine-based model β hairpin and the second β hairpin of the B1 domain of an immunoglobulin G-binding protein from group G *Streptococcus* in liquid water. By using the generalized Hessian matrix reconstruction method, both the directions and magnitudes of all 17 local mode transition dipoles in the A_{17} β hairpin were obtained. It turns out that the variations of norms and directions of local mode transition dipoles are rather small. Therefore, the assumption that the local mode transition dipoles are not strongly dependent on the local environment and conformation is quantitatively acceptable in this case.

By calculating the solvation-induced frequency shifts and fluctuations and carrying out instantaneous amide I normal-mode analysis, we obtained the density of state of the one-exciton band and inverse participation ratio spectrum. The IR absorption spectrum in the static limit was calculated by using the dipole strength-weighted density of the state defined in eq 14. The asymmetric and characteristic spectral features of the β hairpin that were studied experimentally and reported previously were reasonably well described by using the INM analysis method.

To properly take into account the motional and exchange narrowing contributions to both IR absorption and 2D IR photon echo spectra, we used time-correlation function formalism. Because of the subpicosecond relaxation component in the frequency−frequency correlation function, the absorption spectrum becomes significantly narrower than that in the static limit. Furthermore, it was shown that as the inverse participation ratio of a given normal mode increases the associated band becomes narrow. The numerically simulated IR absorption spectrum is both quantitatively and qualitatively similar to those of typical β-hairpin solutions. A quantitative analysis of the IR spectrum was performed by deliberately nullifying the local mode transition dipoles in either the turn region or the strand regions. As can be seen in Figure 7d and c, the intense low-frequency peak is determined largely by the normal modes delocalized on the peptides in the two strands (double-stranded antiparallel β-sheet structure), whereas the normal modes localized on the peptides in the turn region are mostly high-frequency ones. We also considered three different isotope-labeled β hairpins. Depending on the isotope-labeled sites, the position and band shape of the isotope peak changes dramatically.

Using the general nonlinear response function formalism, the 2D IR correlation spectra of unlabeled and three isotope-labeled β hairpins in solution were simulated. For the unlabeled A_{17} β hairpin, two diagonal and two off-diagonal (cross) peaks were observed, which are characteristic features already found in the antiparallel β-sheet proteins by Tokmakoff and co-workers. Also, we showed that the entire 2D IR spectrum is almost completely determined by the peptides in the two strands and not by those in the turn region. Furthermore, comparing the

2D spectra of the GB1 β hairpin with those of the A_{17} β hairpin, we confirmed that the overall 1D and 2D IR spectra are determined by the global secondary structure. The 2D IR spectra of isotope-labeled β hairpins were found to be highly sensitive to the positions of isotope-labeled peptides. In other words, one can achieve a great enhancement of frequency resolution by employing the 2D spectroscopic technique. Also, we not only showed what the characteristic features of β hairpin in both IR absorption and 2D IR spectra are but also demonstrated how reliable the computational method combining electronic structure and molecular dynamics simulation methods for numerically calculating various linear and nonlinear spectra of polypeptides is.

Acknowledgment. This work was supported by the CRIP grant from KOSEF.

References and Notes

(1) Anfinsen, C. B. *Science* **1973**, *181*, 223−230.
(2) Rooman, M. J.; Wodak, S. J. *Biochemistry* **1992**, *31*, 10239−10249.
(3) Rooman, M. J.; Kocher, J.-P. A.; Wodak S. J. *Biochemistry* **1992**, *31*, 10226−10238.
(4) Espinosa, J. F.; Munoz, V.; Gellman, S. H. *J. Mol. Biol.* **2001**, *306*, 397−402.
(5) Bryant, Z.; Pande, V. S.; Rokhsar, D. S. *Biophys. J.* **2000**, *78*, 584−589.
(6) Saxena, V. P.; Wetlaufer, D. B. *Biochemistry* **1970**, *9*, 5015−5023.
(7) Wetlaufer, D. B. *Proc. Natl. Acad. Sci. U.S.A.* **1973**, *70*, 697−701.
(8) Rotondi, K. S.; Gierasch, L. M. *Biochemistry* **2003**, *42*, 7976−7985.
(9) Munoz, V.; Henry, E. R.; Hofrichter, J.; Eaton, W. A. *Proc. Natl. Acad. Sci. U.S.A.* **1998**, *95*, 5872−5879.
(10) McCallister, E. L.; Alm, E.; Baker, D. *Nat. Struct. Biol.* **2000**, *7*, 669−673.
(11) Ramirez-Alvarado, M.; Blanco, F. J.; Niemann, H.; Serrano, L. *J. Mol. Biol.* **1997**, *273*, 898−912.
(12) Blanco, F. J.; Jimenez, M. A.; Herranz, J.; Rico, M.; Santoro, J.; Nieto, J. L. *J. Am. Chem. Soc.* **1993**, *115*, 5887−5888.
(13) Espinosa, J. F.; Syud, F. A.; Gellman, S. H. *Protein Sci.* **2002**, *11*, 1492−1505.
(14) Blanco, F. J.; Rivas, G.; Serrano, L. *Nat. Struct. Biol.* **1994**, *1*, 584−590.
(15) Pande, V. S.; Rokhsar, D. S. *Proc. Natl. Acad. Sci. U.S.A.* **1999**, *96*, 9062−9067.
(16) Garcia, A. E.; Sanbonmatsu, K. Y. *Proteins: Struct., Funct., Bioinf.* **2001**, *42*, 345−354.
(17) Dinner, A. R.; Lazaridis, T.; Karplus, M. *Proc. Natl. Acad. Sci. U.S.A.* **1999**, *96*, 9068−9073.
(18) Kobayashi, N.; Honda, S.; Yoshii, H.; Munekata, E. *Biochemistry* **2000**, *39*, 6564−6571.
(19) Hilario, J.; Kubelka, J.; Keiderling, T. A. *J. Am. Chem. Soc.* **2003**, *125*, 7562−7574.
(20) Honda, S.; Kobayashi, N.; Munekata, E. *J. Mol. Biol.* **2000**, *295*, 269−278.
(21) Arrondo, J. L. R.; Blanco, F. J.; Serrano, L.; Goni, F. M. *FEBS Lett.* **1996**, *384*, 35−37.
(22) Colley, C. S.; Griffiths-Jones, S. R.; George, M. W.; Searle, M. S. *Chem. Commun.* **2000**, *7*, 593−594.
(23) Xu, Y.; Oyola, R.; Gai, F. *J. Am. Chem. Soc.* **2003**, *125*, 15388−15394.
(24) Fang, C.; Wang, J.; Kim, Y. S.; Charnley, A. K.; Barber-Armstrong, W.; Smith, A. B., III; Decatur, S. M.; Hochstrasser, R. M. *J. Phys. Chem. B* **2004**, *108*, 10415−10427.
(25) (a) Demirdoven, N.; Cheatum, C. M.; Chung, H. S.; Khalil, M.; Knoester, J.; Tokmakoff, A. *J. Am. Chem. Soc.* **2004**, *126*, 7981−7990. (b) Cheatum, C. M.; Tokmakoff, A.; Knoester, J. *J. Chem. Phys.* **2004**, *120*, 8201−8215.
(26) Ge, N.-H.; Zanni, M. T.; Hochstrasser, R. M. *J. Phys. Chem. A* **2002**, *106*, 962−972.
(27) Zanni, M. T.; Ge, N.-H.; Kim, Y. S.; Hochstrasser, R. M. *Proc. Natl. Acad. Sci. U.S.A.* **2001**, *98*, 11265−11270.
(28) (a) Bredenbeck, J.; Helbing, J.; Behrendt, R.; Renner, C.; Moroder, L.; Wachtveitl, J.; Hamm, P. *J. Phys. Chem. B* **2003**, *107*, 8654−8660. (b) Bredenbeck, J.; Hamm, P. *J. Chem. Phys.* **2003**, *119*, 1569−1578.
(29) Krummel, A. T.; Mukherjee, P.; Zanni, M. *J. Phys. Chem. B* **2003**, *107*, 9165−9169.
(30) Lee, C.; Cho, M. *J. Phys. Chem. B* **2004**, *108*, 20397−20407.
(31) Choi, J.-H.; Hahn, S.; Cho, M. *Int. J. Quantum Chem.*, in press, 2005.
(32) Torii, H.; Tasumi, M. *J. Chem. Phys.* **1992**, *96*, 3379−3387.
(33) Choi, J.-H.; Ham, S.; Cho, M. *J. Chem. Phys.* **2002**, *117*, 6821−6832.
(34) (a) Ham, S.; Hahn, S.; Lee, C.; Kim, T.-K.; Kwak, K.; Cho, M. *J. Phys. Chem. B* **2004**, *108*, 9333. (b) Lee, H.; Kim, S.; Choi, J.-H.; Cho, M. *J. Phys. Chem. B* **2005**, *109*, 5331.
(35) Case, D. A.; Pearlman, D. A.; Caldwell, J. W.; Cheatham, T. E., III; Wang, J.; Ross, W. S.; Simmerling, C. L.; Darden, T. A.; Merz, K. M.; Stanton, R. V.; Cheng, A. L.; Vincent, J. J.; Crowley, M.; Tsui, V.; Gohlke, H.; Radmer, R. J.; Duan, Y.; Pitera, J.; Massova, I.; Seibel, G. L.; Singh, U. C.; Weiner, P. K.; Kollman, P. A. *AMBER 7*; University of California: San Francisco, 2002.
(36) Darden, T.; York, D.; Pedersen, L. *J. Chem. Phys.* **1993**, *98*, 10089−10092.
(37) Berendsen, H. J. C.; Postma, J. P. M.; van Gunsteren, W. F.; DiNola, A.; Haak, J. R. *J. Chem. Phys.* **1984**, *81*, 3684−3690.
(38) Ham, S.; Kim, J.-H.; Lee, H.; Cho, M. *J. Chem. Phys.* **2003**, *118*, 3491−3498.
(39) Kwac, K.; Cho, M. *J. Chem. Phys.* **2003**, *119*, 2247−2255.
(40) Kwac, K.; Cho, M. *J. Chem. Phys.* **2003**, *119*, 2256−2263.
(41) Kwac, K.; Lee, H.; Cho, M. *J. Chem. Phys.* **2004**, *120*, 1477−1490.
(42) Zanni, M. T.; Asplund, M. C.; Hochstrasser, R. M. *J. Chem. Phys.* **2001**, *114*, 4579−4590.
(43) Woutersen, S.; Pfister, R.; Hamm, P.; Mu, Y.; Kosov, D. S.; Stock, G. *J. Chem. Phys.* **2002**, *117*, 6833−6840.
(44) Woutersen, S.; Mu, Y.; Stock, G.; Hamm, P. *Chem. Phys.* **2001**, *266*, 137−147.
(45) Bayly, C. I.; Cieplak, P.; Cornell, W. D.; Kollman, P. A. *J. Phys. Chem.* **1993**, *97*, 10269.
(46) The *A*-mode-like normal mode refers to the normal modes having all of the eigenvector elements the same sign (in phase). However, the signs of the eigenvector elements of the E_1-mode-like normal mode alternate, meaning that the eigenvector elements of the nearest neighboring local amide I modes are out of phase with each other. On the basis of this notion, there have been numerous attempts to quantitatively determine the frequency splitting between these two (*A*-mode-like and E_1-mode-like) types of normal modes. See Krimm, S.; Reisdorf, W. C., Jr. *Faraday Discuss.* **1994**, *99*, 181 and Torii, H.; Tasumi, M. *J. Chem. Phys.* **1992**, *97*, 86.
(47) Hilario, J.; Kubelka, J.; Syud, F. A.; Gellman, S. H.; Keiderling, T. A. *Biopolymers*, **2002**, *67*, 233−236.
(48) Cho, M. *J. Chem. Phys.* **2001**, *115*, 4424−4437.
(49) Mukamel, S. *Annu. Rev. Phys. Chem.* **2000**, *51*, 691−729.
(50) Wright, J. C. *Int. Rev. Phys. Chem.* **2002**, *21*, 185−255.
(51) Tokmakoff, A. *J. Phys. Chem. A* **2000**, *104*, 4247−4255.
(52) Khalil, M.; Demirdoven, N.; Tokmakoff, A. *J. Phys. Chem. A* **2003**, *107*, 5258−5279.